INL/CON-15-37225
PREPRINT

DETERMINATION OF THE CREEP–FATIGUE INTERACTION DIAGRAM FOR ALLOY 617

EPRI 2016 Creep Fatigue Workshop In Collaboration with ASME PVP

J. K. Wright, L. J. Carroll, T. -L. Sham,
N. J. Lybeck, R. N. Wright

August 2016

The INL is a
U.S. Department of Energy
National Laboratory
operated by
Battelle Energy Alliance

Proceedings of the ASME 2016 Pressure Vessels and Piping Conference
PVP2016
July 17-21, 2016, Vancouver, British Columbia, Canada

PVP2016-63704

DETERMINATION OF THE CREEP–FATIGUE INTERACTION DIAGRAM FOR ALLOY 617

J. K. Wright
Idaho National Laboratory
Idaho Falls, ID, USA

L. J. Carroll
Idaho National Laboratory
Idaho Falls, ID, USA

T.-L. Sham
Argonne National Laboratory
Lemont, IL, USA

N. J. Lybeck
Idaho National Laboratory
Idaho Falls, ID, USA

R. N. Wright
Idaho National Laboratory
Idaho Falls, ID, USA

ABSTRACT

Alloy 617 is the leading candidate material for an intermediate heat exchanger for the very high temperature reactor (VHTR). As part of evaluating the behavior of this material in the expected service conditions, creep–fatigue testing was performed. The cycles to failure decreased compared to fatigue values when a hold time was added at peak tensile strain. At 850°C, increasing the tensile hold duration continued to degrade the creep–fatigue resistance, at least to the investigated strain–controlled hold time of up to 60 minutes at the 0.3% strain range and 240 minutes at the 1.0% strain range. At 950°C, the creep–fatigue cycles to failure are not further reduced with increasing hold duration, indicating saturation occurs at relatively short hold times. The creep and fatigue damage fractions have been calculated and plotted on a creep–fatigue interaction D–diagram. Test data from creep–fatigue tests at 800 and 1000°C on an additional heat of Alloy 617 are also plotted on the D–diagram.

INTRODUCTION

Alloy 617 is the leading candidate material for an intermediate heat exchanger in a high temperature gas–cooled nuclear reactor, which must operate at expected reactor outlet temperatures of up to 950°C. Predominantly solid solution strengthened, Alloy 617 is a nickel–based alloy with high levels of Cr for oxidation resistance and additions of Co and Mo for strengthening. It also contains low levels of Al and Ti that promote the Ni_3Al γ' precipitates at intermediate temperatures [1]. While several existing nickel–base alloys (e.g., 617, 230, and X) are approved for non–nuclear construction under Section VIII of the American Society of Mechanical Engineers (ASME) Boiler and Pressure Vessel (B&PV) Code, none are currently approved to the desired temperatures under the nuclear construction requirements in Section III [2]. A draft Section III high temperature Code Case was developed for Alloy 617 around 1992 [3]; however it was never completed or approved. One of the primary data needs noted during review of the Code Case was an understanding of the creep–fatigue behavior of the alloy [3]. Creep–fatigue is an integral part of the elevated temperature service portion of Section III of the ASME B&PV Code.

Creep–fatigue is expected to be the primary damage mode for the Very High Temperature Reactor (VHTR) intermediate heat exchanger. Transients during start up and shut down produce cyclic loadings, while the stresses relax during steady power operation inducing creep damage. Creep–fatigue testing (strain–controlled fatigue with a hold time at the peak tensile strain) is performed in a laboratory setting to approximate the expected damage mode. Continuous low cycle fatigue (LCF) testing (i.e., no hold time) was also conducted to provide a baseline for the creep–fatigue behavior. Creep–fatigue results are combined with creep rupture and LCF results to develop a creep–fatigue interaction diagram (aka the ASME D–diagram) for Alloy 617.

Table 1. The composition in wt% of Alloy 617.

	Ni	C	Cr	Co	Mo	Fe	Al	Ti	Si	Cu	Mn	S	B
314626	Bal.	0.05	22.2	11.6	8.6	1.6	1.1	0.4	0.1	0.04	0.1	0.002	0.001
XX2834UK	Bal.	0.08	21.91	11.42	9.78	1.69	0.96	0.34	0.12		0.11	0.001	0.002

MATERIALS

The majority of the fatigue and creep–fatigue testing has been performed on specimens machined from an Alloy 617 reference material plate [4]. The 37 mm thick solution–annealed plate is from heat 314626, produced by ThyssenKrupp VDM and the composition is given in Table 1. Although the average grain size of the plate is quantified as approximately 150 μm, significant grain size inhomogeneity is present in the microstructure.

Additional creep–fatigue tests were performed on specimens machined from a 20 mm thick plate of Alloy 617 (heat XX2834UK) procured from Special Metals Corporation [5,6]. The chemical composition of this plate is also listed in Table 1. The microstructure of this plate is heavily banded with stringers of coarse carbide precipitates and associated coarse and fine grains aligned in the rolling direction. Grains in the coarse bands are approximately 100 μm in diameter and the finer grains range from approximately 10 to 30 μm in diameter.

CREEP–FATIGUE TEST PROCEDURES

Cylindrical cyclic test specimens were machined with the longitudinal axis of the specimens aligned with the rolling direction of the plates. Low stress grinding and longitudinal polishing were used in the final machining of the reduced section to eliminate cold work and circumferential machining marks.

Fully reversed, strain–controlled continuous LCF and creep–fatigue tests were performed in air at total strain ranges from 0.3% to 1.0% on servo–hydraulic test machines. The hold time duration in creep–fatigue varied from as short as 2 seconds to as long as 240 minutes. Testing was designed to be compliant with American Society for Testing and Materials (ASTM) Standard E606 [7]. Tests on heat 314626 were performed at 850 and 950°C [8 - 10], while tests on heat XX2834UK were performed at 800 and 1000°C [5,6]. Specimens were heated either using a 3–zone resistance furnace or by induction. The temperature gradient was measured using a specimen with spot welded thermocouples along the gage section, and was found to vary less than 1%, as specified in E606. Temperature was typically controlled to within 1% of the target temperature; some specimens tested at 950°C and subjected to 1% total strain range had temperature variations of 2-2.5% because of movement of the control thermocouple relative to the induction coil. LCF testing followed a triangular waveform. The majority of creep–fatigue testing employed a tensile hold waveform with a strain–controlled hold time at the peak tensile strain, although a few tests were performed with compressive, or tensile and compressive holds. The strain rate during loading and unloading was 10^{-3} /s, except for selected tests which had a strain rate of 4×10^{-4} /s. In some cases the total strain range was incrementally increased over a limited number of initial cycles prior to achieving the target strain range, in order to prevent overshooting the target strain. Additionally, in some tests the waveform was modified to smooth the transition from the ramp to the hold period, which minimizes the amount that the target strain is exceeded.

The number of cycles to failure, N_f, is determined from a plot of the ratio of peak tensile to peak compressive stress versus cycles, as originally described in Ref. [5]. Determining the life from this ratio allows changes in peak stresses due to cyclic hardening or softening to be distinguished from those due to crack formation and propagation. Macro-crack initiation is defined as the point at which the stress ratio deviated from linearity; failure is defined as a 20% reduction in stress ratio from the point of deviation. Due to the rapidly falling peak tensile force during the final crack propagation phase, N_f is not particularly sensitive to the exact value of load drop used to define failure or to the accuracy of the macro–crack initiation determination.

In most cases, test termination was prior to actual specimen separation, based upon a predetermined drop in load. When the set load drop was detected, the test automatically switched to zero load and power to the heat source was shut off. Selected specimens were examined after testing to reveal the cracking morphology. Transverse sections of the gage length were prepared and examined using standard metallographic techniques.

CREEP–FATIGUE INTERACTION ANALYSIS

In the ASME Code, creep–fatigue life is evaluated by a linear summation of fractions of cyclic damage and creep damage. The creep–fatigue criterion is given by:

$$\underbrace{\sum_j \left(\frac{n}{N_d}\right)_j}_{\text{Cyclic Damage}} + \underbrace{\sum_k \left(\frac{\Delta t}{T_d}\right)_k}_{\text{Creep Damage}} \leq D \qquad (1)$$

where n and N_d are the number of cycles of type j and the allowable number of cycles of the same cycle type, respectively; and Δt and T_d are the actual time at stress level k and the allowable time at that stress level, respectively; D is the allowable combined damage fraction. Since the creep damage term is evaluated as a ratio of the actual time versus the allowable time, it is generally referred to as a time–fraction. The cyclic and creep damage terms on the left hand side of Equation (1) are evaluated in an uncoupled manner, and the interaction of creep and fatigue is accounted for empirically by

the *D* term on the right side of the equation. This is represented graphically by the creep–fatigue interaction diagram, which is shown for the ASME Section III Division 5 materials in Figure HBB-T-1420-2, reproduced here as Figure 1. The bilinear curves represent the damage envelopes for each material, within which calculated damage for a design must fall.

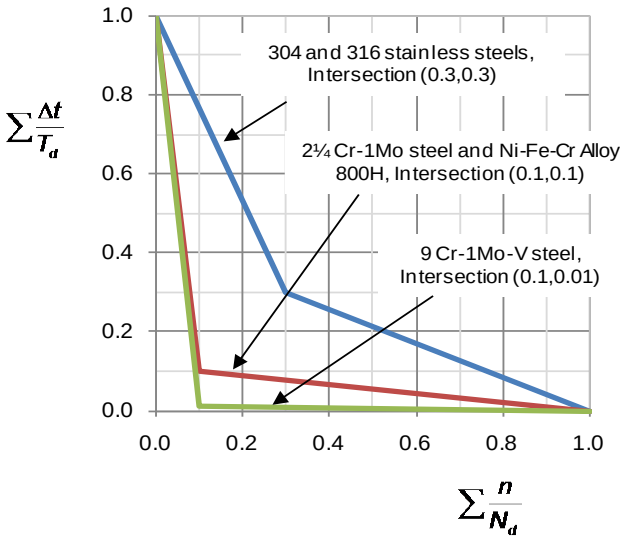

Figure 1. Creep–fatigue interaction diagram for ASME Section III, Division 5, Subsection HB, Subpart B. The coordinates of the intersections of the bilinear curves are shown in the legend.

Fatigue Damage Calculations

The fatigue damage fraction, D_F, for a creep–fatigue test is defined in terms of the ratio of the cycle to failure under the creep–fatigue condition, N_f, to the cycle to failure under continuous cycling condition, N_d, for the same product form and heat, and at the same total strain range, strain rate, and temperature as the creep–fatigue test. If data for more than one continuous cycling test for the same set of conditions were obtained, their average was used for the value of N_d, as best estimate values are to be used for establishing the envelope of the interaction curve in the D–diagram. For each creep–fatigue test, there was at least one LCF test for the same conditions.

Creep Damage Calculations

Development of Equations

The creep damage for the k^{th} creep–fatigue cycle, D_k^c, can be determined by evaluating the integral

$$D_k^c = \int \left(\frac{1}{T_d}\right)_k dt \qquad (2)$$

over the hold time of the cycle.

To perform the integration, the correlation between the rupture time, temperature, and applied stress for the heat of Alloy 617 under consideration is required. In this analysis, a creep rupture time correlation based on all available creep rupture data for Alloy 617 was used in the creep damage evaluation. A Larson–Miller relation is a common way to do this and for Alloy 617, a linear equation in log stress describes the creep data well [11].

$$LMP = a_0 + a_1 log_{10}(\sigma) \qquad (3)$$

where a_0 and a_1 are the fitting parameters, σ is stress (MPa) and *LMP* is the Larson–Miller Parameter, defined as

$$LMP = T\left(C + log_{10}(t)\right) \qquad (4)$$

and T is the temperature in Kelvin, C is the Larson–Miller constant, and t is time in hours.

Isolating t on the left side, we have

$$log_{10}(t) = -C + \frac{a_0}{T} + \frac{a_1}{T} log_{10}(\sigma) \qquad (5)$$

and changing the base to the natural logarithm gives

$$\frac{ln(t)}{ln(10)} = -C + \frac{a_0}{T} + \frac{a_1}{T}\frac{ln(\sigma)}{ln(10)} \qquad (6)$$

which can be rearranged as

$$\ln(t) = -C\, ln(10) + \frac{a_0\, ln(10)}{T} + \frac{a_1 ln(\sigma)}{T} \qquad (7)$$

Hence

$$t = \exp\left(-C \ln(10) + \frac{a_0 \ln(10)}{T}\right)\sigma^{\left(\frac{a_1}{T}\right)} \qquad (8)$$

or

$$t = 10^{\left(-C+\frac{a_0}{T}\right)}\sigma^{\left(\frac{a_1}{T}\right)} \qquad (9)$$

For the calculations that follow, it is more convenient to use time in seconds for T_d, so we have:

$$T_d = 3600 * 10^{\left(-C+\frac{a_0}{T}\right)}\sigma^{\left(\frac{a_1}{T}\right)} \qquad (10)$$

We can rewrite (10) as

$$T_d = \mathrm{A}\sigma^m \qquad (11)$$

where

$$A = 3600 * 10^{\left(-C+\frac{a_0}{T}\right)}, \quad m = \frac{a_1}{T} \qquad (12)$$

The damage for a given cycle is calculated by integrating $\frac{1}{T_d}$ over the hold time. This requires analysis of the stress as it relaxes during the strain hold period, which can be fit to a power–law trend curve using the following functional form:

$$\sigma = b_0(t + t_0)^{b_1} \qquad (13)$$

where b_0, b_1, and t_0 are treated as fitting parameters, σ is stress in MPa and t and t_0 are in seconds.

Substituting Equations (11) - (13) into Equation (2) results in

$$D_k^c = \int_0^{t_h} \frac{1}{A}\left(b_0(t + t_0)^{b_1}\right)^{-m} dt \qquad (14)$$

$$D_k^c = \frac{{b_0}^{-m}}{A}\frac{(t+t_0)^{1-b_1 m}}{1-b_1 m}\Big|_0^{t_h} \qquad (15)$$

$$D_k^c = \frac{{b_0}^{-m}}{A(1-b_1 m)}\left((t_h + t_0)^{1-b_1 m} - (t_0)^{1-b_1 m}\right) \qquad (16)$$

where t_h is the stress relaxation hold time in seconds. The total creep damage accumulated during a creep–fatigue test, D_C, can then be determined by summing the creep damages calculated for all the cycles. This would require the stress relaxation for each cycle. However, such data are not collected for all the cycles during a creep–fatigue test. An approximation commonly made in calculating the total creep damage is to evaluate the creep damage for one cycle close to the midlife, and then multiply this value by the total number of cycles to failure in the creep–fatigue test.

The Larson–Miller Relation

A Larson–Miller relation for time to creep–rupture was developed using a data set comprised of information from 348 creep–rupture specimens from multiple heats and product forms with known chemistry. For one of the heats described here (XX2834UK), cycles to failure in fatigue was determined as part of the creep–fatigue testing, but creep–rupture tests were not performed, so the creep damage fraction could not be determined using a heat–specific Larson–Miller relation. Using the Alloy 617 Larson–Miller equation from the complete data set enabled integration of the maximum number of creep–fatigue tests onto the interaction diagram.

A spreadsheet developed for ASME [11] for analysis of time–dependent materials properties was used to generate the Larson–Miller relation (Figure 2). Regression analysis for a linear fit produced values of

a_0 = 32976.41125

a_1 = -5908.103107

C = 16.73049602

according to Equations (3) and (4).

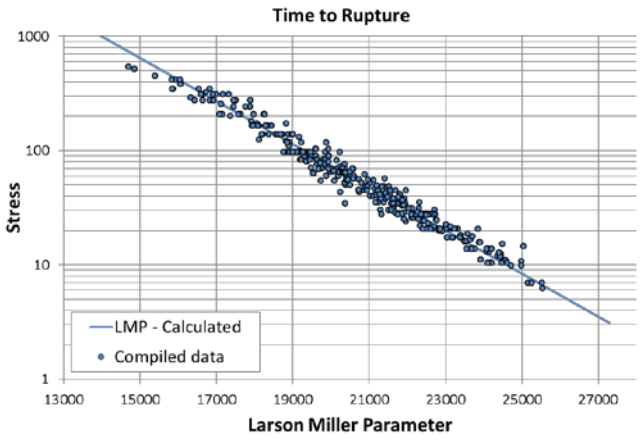

Figure 2. Larson–Miller plot with a linear fit for time to creep rupture of Alloy 617.

Analysis of Stress Relaxation

The stress relaxation curves during the strain hold for midlife cycles were fit to Equation (11) and the fitting parameters were determined for a cycle close to midlife for each creep–fatigue test. These parameters are used with the equations developed above to evaluate the creep damage for those selected cycles. An example of the power-law fit to midlife stress relaxation data during the strain hold period is shown in Figure 3.

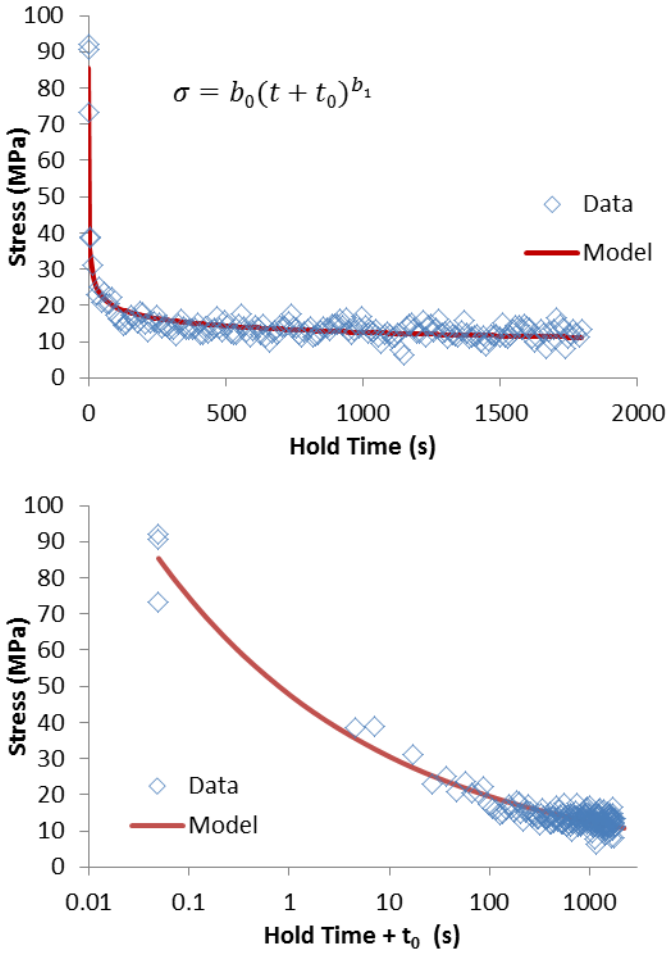

Figure 3. Example of a power law fit to the stress relaxation portion of the midlife creep–fatigue cycle of an Alloy 617 specimen cycled at 950ºC, 0.3% total strain, and 1800 s hold time, plotted in both linear and semi-log scale.

RESULTS

Creep–fatigue Behavior

For the fatigue and tensile–hold creep–fatigue testing of Alloy 617 conducted at 950 and 1000ºC, the cycles to failure as a function of hold time are shown in Figure 4 for the 1×10^{-3} /s strain rate test data from multiple sources [5,8-10]. The 950°C data sets are self–consistent in terms of cycles to failure [8-10], and also are consistent with the data of Rao et al. at 0.6% strain in simulated primary–circuit helium gas [12], and of Totemeier at 1000°C [5]. As previously reported for Alloy 617 [5-9,12], the addition of a tensile hold time in creep–fatigue decreased the total cycle life. The cycle lifetimes for creep–fatigue versus continuous–cycle fatigue are reduced by roughly a factor of 2 for all three of the strain ranges.

Saturation, defined as the point at which further increases in the hold time duration no longer decrease the cycle life, is apparent for Alloy 617 at 950°C at least to hold times of 30 mins [8,9]. The challenging nature of long hold durations at high temperatures results in a minimal amount of data with hold times longer than 30 mins. The data that is available at both 950 and 1000°C indicates that the determination of saturation at very long hold times is not straightforward; two data points indicate saturation and two indicate no saturation.

The creep–fatigue saturation behavior of Alloy 617 was also investigated at lower temperatures, 800 and 850°C, primarily at 0.3 and 1.0% total strain range [6,10,13]. The cycles to failure are plotted as a function of hold time in Figure 5. The addition of a strain–controlled tensile hold decreases the total number of cycles to failure relative to LCF. A dramatic degradation in cycle life occurs with the addition of a short hold time at the 0.3% total strain range. This drop in cycle life is more substantial than that observed for short hold times at the 0.6 or 1.0% strain range. The number of cycles to failure progressively decreases with longer hold times for both the 0.3 and 1.0% strain ranges for the investigated hold durations of up to 60 and 240 minutes, respectively. Although the 800°C data does appear to saturate at the 1.0% strain range for the moderate duration hold times tested [6], in general, the available data indicates that saturation is not observed at 800 or 850 °C.

The dramatic difference in the number of cycles to failure between fatigue and creep–fatigue at the 0.3% strain range is consistent with the characteristically different hysteresis loops. For LCF, the stress–strain loop is narrow with limited inelastic behavior; however, the 30–minute–hold loop is approximately three times wider, exhibiting substantially more inelastic strain, as shown Figure 6. The inelastic strain increases with increasing hold time consistent with the fact that the stresses do not fully relax during the strain–controlled hold, as shown in the schematic of the midlife cycle stress relaxation behavior of a selected 0.3% strain range test in Figure 7(a). In other words, the stress at the end of the hold time continues to decrease with increasing hold duration. Rapid stress relaxation is also observed at the 1.0% total strain range, shown for the 240–minute hold time condition in Figure 7(b); however, the stresses plateau by hold times of approximately 120 minutes.

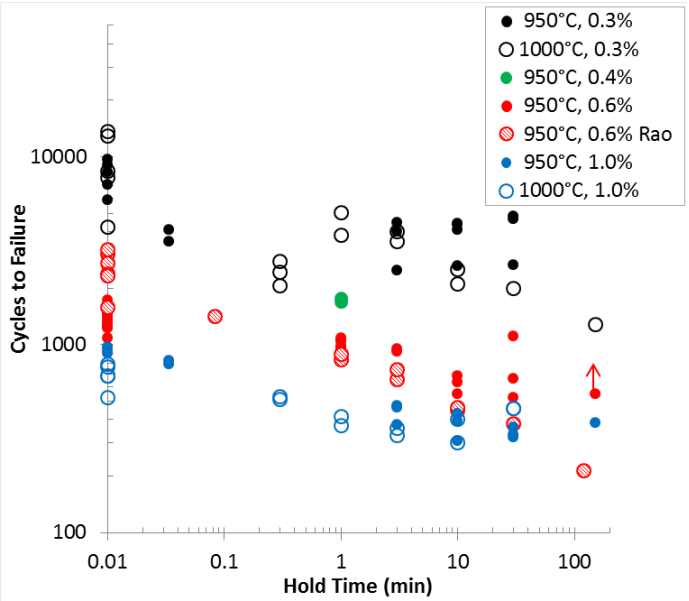

Figure 4. The number of cycles to failure as a function of hold time in fatigue and creep–fatigue of Alloy 617 at 950 and 1000°C at various total strain ranges. (Red arrow indicates a test that was stopped before failure.)

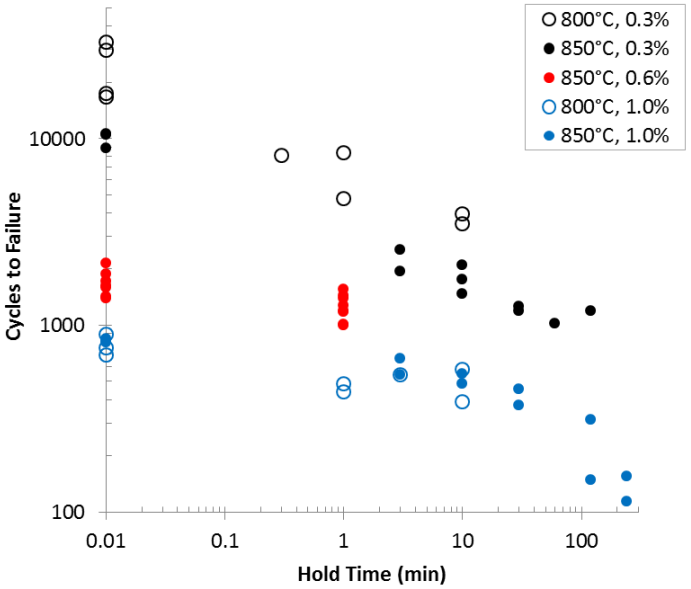

Figure 5. The number of cycles to failure as a function of hold time in fatigue and creep–fatigue of Alloy 617 at 800 and 850°C at various total strain ranges.

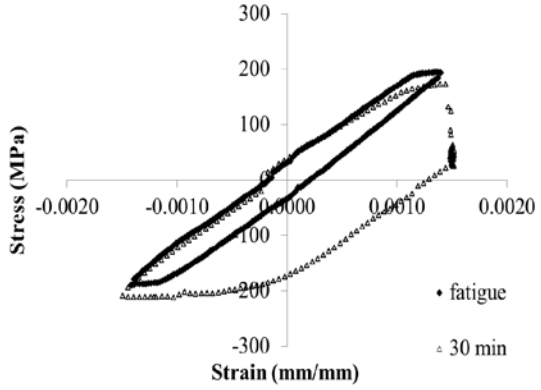

Figure 6. Midlife fatigue and 30-minute hold creep–fatigue hysteresis loops from selected tests at 850°C and 0.3% total strain.

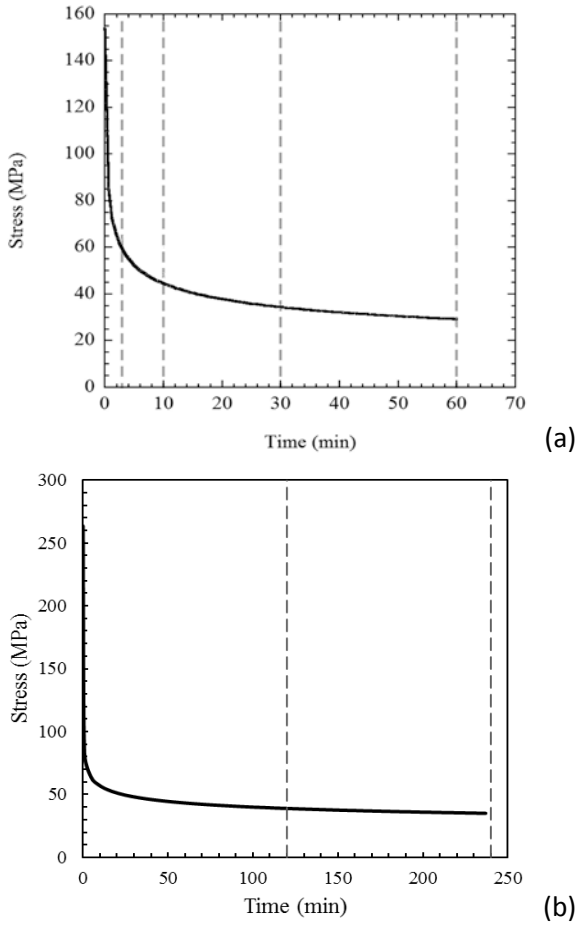

Figure 7. Midlife stress relaxation at 850°C during the peak tensile strain–controlled hold time of a) 60 minutes at 0.3% total strain and b) 240 minutes at 1.0% total strain.

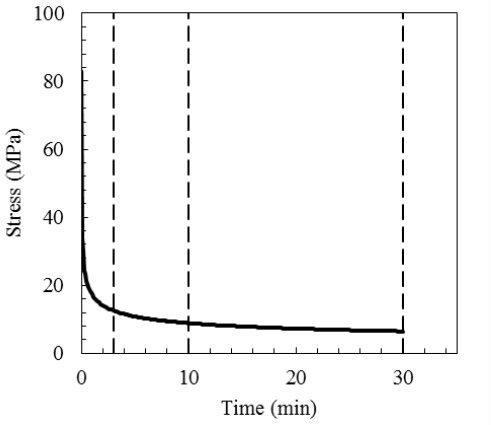

Figure 8. A midlife stress relaxation fit for the peak tensile strain–controlled hold time of 30 minutes at 950°C and 0.3% total strain.

The difference in saturation behavior between the higher (950 and 1000°C) and lower (800 and 850°C) creep–fatigue tests can also be understood in terms of the differences in stress relaxation behavior. At 850°C, stress relaxation during the strain–controlled tensile hold (Figure 7) exhibits higher initial stresses and higher relaxed stresses than at 950°C (Figure 8). Additionally at 850°C, the stresses continually decrease with time throughout the hold (with the exception of the longest hold time condition, 240 minutes, for the 1.0% strain range), while stresses at 950°C relaxed rapidly and reached a fully relaxed stress at short times. The rapid stress relaxation at 950°C was observed regardless of strain range or hold time. As a result, the material is subjected to a relatively low stress level during the tensile hold, and the creep damage appears to be less detrimental to specimen life than at 850°C. The additional tensile hold time at these low stress levels results in little additional creep damage as calculated for the D–diagram using Equation (16).

Crack Morphology

In general, two crack phenomena are observed from the addition of a tensile hold that result in fewer cycles to failure than observed for LCF: earlier crack initiation occurring at surface–connected grain boundaries that have become oxidized and faster crack propagation resulting from the linking of extensive interior grain boundary cracking [9]. The occurrence of oxidized surface cracks and interior grain boundary cracking varies with creep–fatigue condition.

At 800°C, surface–initiated transgranular cracking is observed for both LCF and creep–fatigue tests with hold times of 1 and 10 minutes. Intergranular cavities were observed in coarse–grained areas in tests with tensile hold periods, but these cavities did not clearly interact with the primary crack leading to failure [6]. At 850°C, cycling in fatigue results in primary transgranular surface cracks (Figure 9a), with no evidence of interior grain boundary cavitation or cracking. Creep–fatigue cycling produces interior grain boundary cracking and crack

propagation evolves from mixed–mode to intergranular as the hold time is increased (Figure 9b). This transition occurs at shorter hold times for the 1% than for the 0.3% total strain range, as shown in Table 2 [13].

Intergranular crack initiation and propagation is observed in all of the creep–fatigue specimens cycled at 950 and 1000°C, regardless of strain range [6,8]. Interior grain boundary cracking was observed to be prevalent throughout the gage section at 950 °C, as shown in Figure 10 [8,9] and grain boundary cavitation was reported in creep–fatigue specimens tested at 1000°C [5]. LCF resulted in primary transgranular surface cracks at 950°C [8], but initiated at oxidized grain boundaries at 1000°C [5].

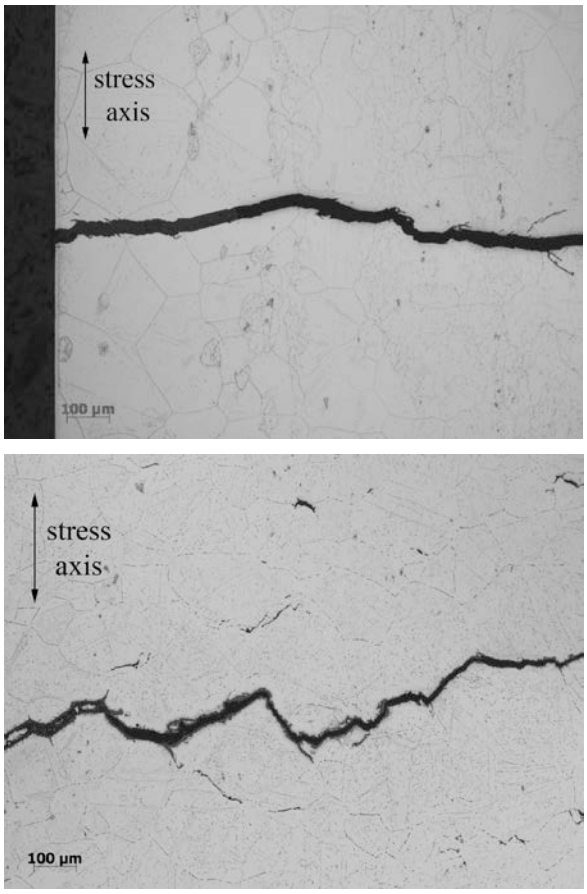

Figure 9. a) A transgranular surface crack in a 0.3% total strain fatigue specimen cycled at 850ºC and b) an intergranular surface crack in a 0.3% total strain, 30-minute hold creep–fatigue specimen cycled at 850ºC (the specimen surface in (b) is to the left of the image).

Table 2. Cracking modes observed in fatigue and creep–fatigue specimens tested at 850ºC selected for metallurgical evaluation.

Condition	Primary Cracking Mode	Interior Grain Boundary Cracking
0.3% total strain range		
fatigue	Transgranular	No
3 min.	Mixed	Yes
10 min.	Primarily Intergranular	Yes
30 min.	Intergranular	Yes
60 min.	Intergranular	Yes
1.0% total strain range		
fatigue	Transgranular	No
3 min.	Transgranular	Limited
10 min.	Mixed	Limited
30 min.	Intergranular	Yes
120 min.	Intergranular	Concentrated regions, limited elsewhere
240 min.	Intergranular	Concentrated regions, limited elsewhere

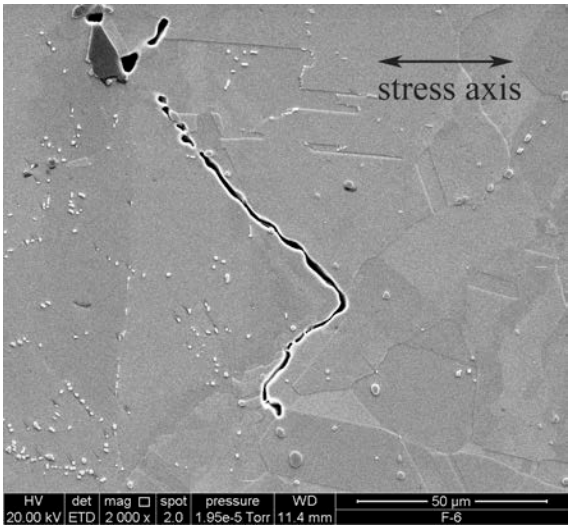

Figure 10. Interior grain boundary cracking observed in a creep–fatigue specimen deformed at 950°C to a total strain range of 0.3% with a 3 minute hold.

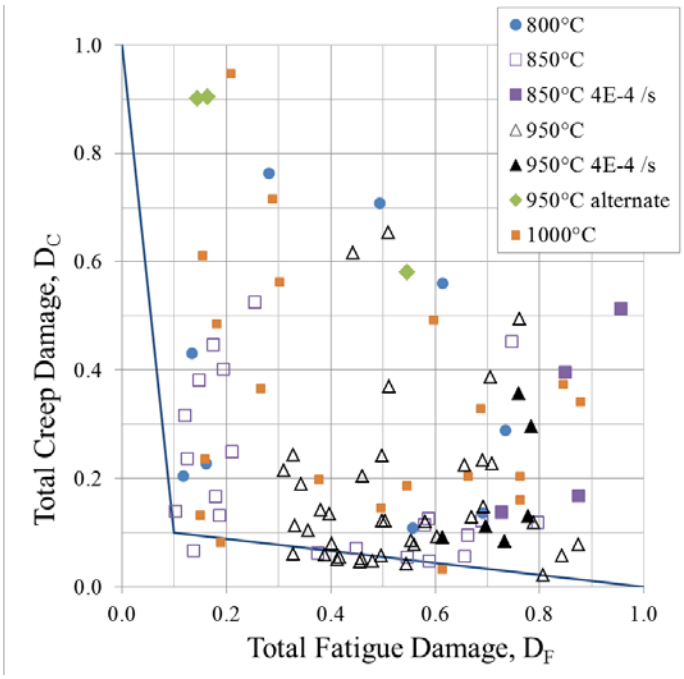

Figure 11. Creep–fatigue data for Alloy 617. The solid line represents the creep–fatigue envelope from the Draft Alloy 617 Code Case 4. The intersection coordinates are (0.1, 0.1).

D–DIAGRAM

The creep damage and fatigue damage fractions for all the creep–fatigue tests are depicted in the creep–fatigue interaction diagram shown in Figure 11. The strain rate for all tests was 10^{-3} /s unless specified otherwise in the legend, and "alternate" refers to tests that had a compressive hold or both tensile and compressive holds. The creep–fatigue damage envelope with an intersection point of (0.1, 0.1), as proposed for Alloy 617 by Corum and Blass [3], is also shown in Figure 11. Generally, the creep–fatigue damage envelope is intended to represent the average trend of the interaction between the creep damage and fatigue damage and it can be seen from the figure that this intersection point results in some data points on and below the lower portion of the line. An intersection point of (0.1, 0.1) provides a conservative representation of the data. Alloy 800H, a Fe-Ni-Cr high temperature alloy in the nuclear portion of the ASME B&PV also has an intersection point of (0.1, 0.1) [2].

An in–depth analysis of the creep–fatigue data on the D–diagram indicates that it does group by test condition (although testing at a strain rate of 4×10^{-4} /s rather than 10^{-3} /s does not appear to cause a systematic or substantial difference in placement of points on the D–diagram). Figure 12 shows a subset of the creep–fatigue data tested at 850°C and total strain ranges of 0.3 and 1.0%. The 0.3% data tend to have low D_F values and higher D_C values, while the 1.0% data have lower D_C values and higher D_F values. The inelastic strain experienced during each cycle is substantially increased by the constant–strain hold for tests at the 0.3% strain range, where LCF results in very little inelastic strain (narrow hysteresis loops), as shown in Figure 6. As a consequence, the cycles to failure for the 0.3% creep–fatigue tests are significant decreased compared to the 0.3% LCF tests. For higher strain ranges, even LCF tests experience significant inelastic strain during each cycle (wider hysteresis loops), so the increase in the width of the hysteresis loop resulting from a tensile strain hold is minimal, and cycle life is similar for creep–fatigue and LCF tests. The difference in creep damage is primarily a reflection of the cycle life of a specimen. All 850°C creep–fatigue specimens have creep damage, D_k^c, for the midlife creep–fatigue cycle on the order of 10^{-4}, and this value is multiplied by number of cycles to obtain the total creep damage fraction. Specimens subjected to smaller strain range cycles have longer lives, and therefore more calculated creep damage, D_C. For both strain ranges, longer hold times result in data points closer to the intersection point of the D–diagram, while shorter hold times have higher relative amounts of calculated creep damage for 0.3% total strain or fatigue damage for 1.0% total strain.

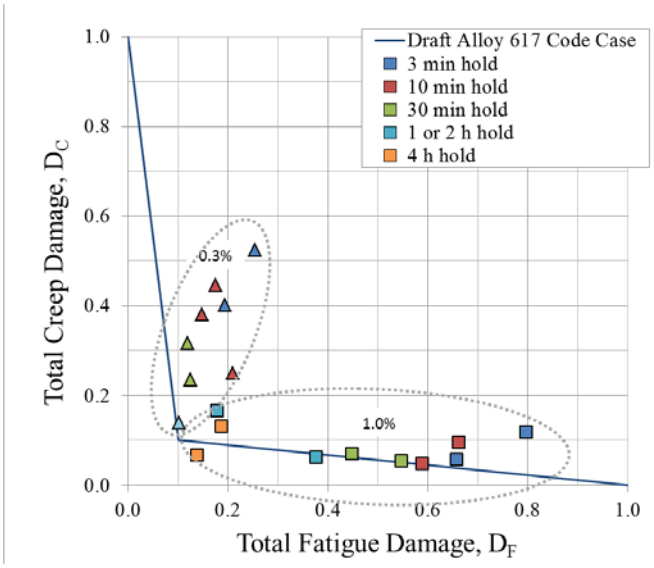

Figure 12. D–diagram for 850°C data tested at total strain ranges of 0.3% (triangles) and 1.0% (squares) with various hold times.

Similar trends can be observed in Figure 13 for the 950°C, 0.3 and 1.0% total strain range tests, although the strain ranges overlap. The effect of hold time on cycle life is only seen for short times, before saturation is indicated, and only the 2 second hold points are clearly outside the overlapping cluster of points in Figure 13.

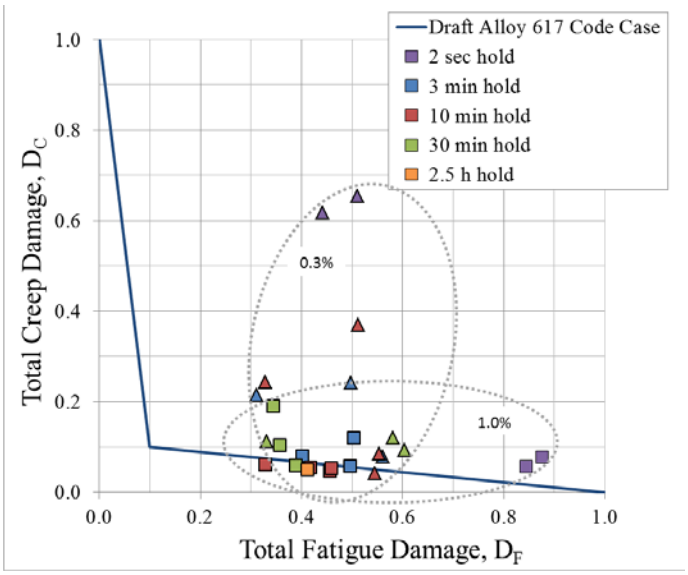

Figure 13. D–diagram for 950°C data tested at total strain ranges of 0.3% (triangles) and 1.0% (squares) with various hold times.

The Alloy 617 testing and development of the D-diagram reported in this paper is intended to support an ASME Code Case to allow use of this material in nuclear construction. As a result, the analysis uses the specified time-fraction approach and consolidates all of the results onto a single D-diagram. Other approaches are possible, including for example the ductility exhaustion approach in the British R5 Code. While it would be interesting to apply those methods to a material such as Alloy 617, that exhibits elastic-plastic behavior with little or no work hardening at these temperatures, it is beyond the scope of the current investigation.

CONCLUSION

Fully reversed, strain–controlled LCF and tensile–hold creep–fatigue testing was conducted in air at total strain ranges from 0.3% to 1.0%, temperatures from 800-1000°C, and over a range of hold times as short as 2 seconds and as long as 4 hours. The creep and fatigue damage fractions have been calculated for all creep–fatigue tests and results have been plotted to determine the creep–fatigue interaction D–diagram. A few tests with compression holds and others with a slightly slower strain rate were also plotted on the D–diagram. The coordinates of the intersection point of the damage envelope is recommended as (0.1, 0.1).

At 950°C, the creep–fatigue cycles to failure is not degraded further with increasing hold time duration, indicating saturation occurs at relatively short hold times. However, at 850°C increases in the tensile hold duration degrade the creep–fatigue resistance, at least to the investigated hold times of up to 60 minutes at the 0.3% strain range and 240 minutes at the 1.0% strain range.

Fracture mode evolves from transgranular for LCF to intergranular with increasing tensile hold time at 850°C. Fracture mode is generally transgranular at 800°C and intergranular for the higher temperatures studied.

At 850°C, the 0.3% strain range data tend to have low D_F (fatigue damage fraction) values. The inelastic strain experienced during each cycle is substantially increased by the constant–strain hold over that experienced for LCF, resulting in a significant decrease in cycles to failure for the creep–fatigue tests. The 1.0% strain range data have higher D_F values because the LCF tests experience significant inelastic strain during each cycle, so the addition of a hold has a smaller impact on cycle life. All 850°C creep–fatigue specimens have midlife creep damage values of the same order of magnitude, and this value is multiplied by number of cycles to obtain the total creep damage fraction, so the cycle life governs the creep damage calculation. Specimens subjected to smaller strain range cycles naturally have longer lives and therefore higher D_C values. Hold time impacts both the fatigue and creep damage fraction. Similar trends on the D–diagram can be observed for the 950°C tests, although data points are less differentiated. The effect of hold time is only seen for short times, before saturation occurs.

ACKNOWLEDGMENTS

The authors would like to thank Bob Jetter for thoughtful guidance and discussions regarding this subject matter. The authors would also like to acknowledge Joel Simpson and Randy Lloyd for conducting the creep–fatigue testing, Thomas Lillo and Julian Benz for conducting the creep testing, and Tammy Trowbridge and Todd Morris for metallurgical work required for this study.

This work was supported through the U.S. Department of Energy Office of Nuclear Energy. This manuscript has been co-authored by Battelle Energy Alliance, LLC under Contract No. DE-AC07-05ID14517, and by UChicago Argonne LLC under Contract No. DE-AC02-06CH11357, with the U.S. Department of Energy. The United States Government retains and the publisher, by accepting the article for publication, acknowledges that the United States Government retains a nonexclusive, paid–up, irrevocable, world–wide license to publish or reproduce the published form of this manuscript, or allow others to do so, for United States Government purposes.

REFERENCES

[1] Wu, Q., Song, H., Swindeman, R. W., Shingledecker, J. P., and Vasudevan, V. K., "Microstructure of Long-Term Aged IN617 Ni-Base Superalloy," *Metallurgical and Materials Transactions*, **39A**, 2008, pp. 2569-85.

[2] ASME, 2015, *ASME Boiler and Pressure Vessel Code, Section III, Division 5*, "Rules for Construction of Nuclear Facility Conponents, High Temperature Reactors," ASME, New York.

[3] Corum, J. M., and Blass, J. J., "Rules for Design of Alloy 617 Nuclear Components to Very High Temperatures,"

PVP Pressure Vessel Piping Fatigue Fracture and Risk ASME, **215**, 1991, pp. 147–153.

[4] Wright, J. K., Carroll, L. J., Cabet, C., Lillo, T. M., Benz, J. K., Simpson, J. A., Lloyd, W. R., J. A. Chapman, and Wright, R. N. "Characterization of Elevated Temperature Properties of Heat Exchanger and Steam Generator Alloys," *Nuclear Engineering Design*, **251**, 2012, pp. 252–260.

[5] Totemeier, T. and Tian H., "Creep–Fatigue-Environment Interactions in Inconel 617," *Materials Science and Engineering A*, **468-470**, 2007, pp. 81-87.

[6] Totemeier, T. C., "High-Temperature Creep–Fatigue of Alloy 617 Base Metal and Weldments", *Proceedings of CREEP8, Eighth International Conference on Creep and Fatigue at Elevated Temperatures, San Antonio, TX, July 22-26*, 2007.

[7] Standard Test Method for Strain–Controlled Fatigue Testing, ASTM E606/E606M-12, ASTM International, West Conshohocken, PA.

[8] Carroll, L. J., Cabet, C., Carroll, M. C., and Wright, R. N., "The Development of Microstructural Damage During High Temperature Creep–fatigue of a Nickel Alloy," *International Journal of Fatigue*, **47A**, 2013, pp. 115-125.

[9] Carroll, M. C., and Carroll, L. J., "Developing Dislocation Subgrain Structures and Cyclic Softening During High-Temperature Creep–Fatigue of a Nickel Alloy," *Metallurgical and Materials Transactions*, **44** (8), 2013, pp. 3592-3607.

[10] P. G. Pritchard, L. Carroll, T. Hassan, "Constitutive Modeling of High Temperature Uniaxial Responses of Alloy 617," *Transactions of the American Nuclear Society*, **109**, 2013, pp. 562-565.

[11] Swindeman, R. W., and Swindeman, M. J., *Analysis of Time-Dependent Materials Properties Data*, ASME Standards Technology, LLC, 2014.

[12] Rao, K. B. S., Meurer, H. P., and Schuster, H., 1988, "Creep–Fatigue Interaction of Incontel 617 at 950°C in Simulated Nuclear Reactor Helium, *Materials Science and Engineering*, **104**, pp. 37-51.

[13] Carroll, L. "Progress Report on Long Hold–time Creep–fatigue of Alloy 617 at 850°C," INL/EXT-15-35132 Rev. 1, August 2015.